EUROPEAN ORGANIZATION FOR NUCLEAR RESEARCH (CERN)

CERN-EP-2019-ZZZ
LHCb-PAPER-2019-034
October 22, 2019

Observation of the semileptonic decay $B^+ \to p\bar{p}\mu^+\nu_\mu$

LHCb collaboration[†]

Abstract

The Cabibbo-suppressed semileptonic decay $B^+ \to p\bar{p}\mu^+\nu_\mu$ is observed for the first time using a sample of pp collisions corresponding to an integrated luminosity of 1.0, 2.0 and 1.9 fb^{-1} at centre-of-mass energies of 7, 8 and 13 TeV, respectively. The differential branching fraction is measured as a function of the $p\bar{p}$ invariant mass using the decay mode $B^+ \to (J/\psi \to \mu^+\mu^-)K^+$ for normalisation. The total branching fraction is measured to be

$$\mathcal{B}(B^+ \to p\bar{p}\mu^+\nu_\mu) = (5.27^{+0.23}_{-0.24} \pm 0.21 \pm 0.15) \times 10^{-6},$$

where the first uncertainty is statistical, the second systematic and the third is from the uncertainty on the normalisation branching fraction.

For submission to JHEP

[†]Authors are listed at the end of this paper.

1 Introduction

Studies of semileptonic B meson decays have recently generated interest due to a number of anomalies in experimental results. Measurements of the observables $R(D)$ and $R(D^*)$ [1–6] have shown hints of lepton non-universality with a combined significance of over $3\,\sigma$ [7]. To probe the flavour structure of possible new physics contributions to these decay modes, it is desirable to make analogous measurements for decays involving different quark-level processes, such as $b \to u$ transitions. To that end, the decay mode $B^+ \to p\overline{p}l^+\nu_l$ is promising experimentally, particularly when performing the measurement at a hadron collider. The requirement of a proton anti-proton pair in the final state should significantly reduce combinatorial background, which would otherwise be significant for final states with pions.

Semileptonic decays of B mesons to a final state containing multiple baryons are as yet unobserved. A theoretical model of $B^+ \to p\overline{p}l^+\nu_l$ decays has been constructed with perturbative QCD (pQCD) [8]. This model is based on studies of several fully hadronic $B \to Y\overline{Y}'X$ decays where Y and $\overline{Y}'$ represent baryons and X one or more mesons. By fitting the angular distributions and decay rates of the hadronic modes [9, 10] the authors of these papers estimate the differential rate of the $B^+ \to p\overline{p}l^+\nu_l$ decays. They also predict the total branching fraction of the $B^+ \to p\overline{p}l^+\nu_l$ decay to be $(1.04 \pm 0.38) \times 10^{-4}$ for $l = \mu$, e leptons. This prediction motivated a search by the Belle collaboration for $B^+ \to p\overline{p}l^+\nu_l$ decays [11], who found evidence for the $B^+ \to p\overline{p}e^+\nu_e$ decay mode with $3.0\,\sigma$ significance. The branching fraction was measured to be $(8.2^{+3.7}_{-3.2} \pm 0.6) \times 10^{-6}$, two orders of magnitude smaller than the prediction.

The measurements of the fully hadronic modes show features that merit further investigation. It is surprising that the branching fractions of decays of B mesons to final states comprising only two baryons are suppressed compared to those of two baryons and one or more extra final state particles [12]. For example, the branching fraction of $B^0 \to p\overline{p}$ is two orders of magnitude smaller than that of the similar $B^0 \to p\overline{p}\pi^+\pi^-$ decay [12, 13]. Furthermore, the invariant mass distributions of the baryon pair in $B \to Y\overline{Y}'X$ decays show the so-called threshold enhancement effect. This is a characteristic shape that peaks at low values [14–17]. Understanding the dynamics that leads to such features is difficult in fully hadronic decays, due to the interaction of the two baryons with the extra hadrons. It is therefore desirable to study semileptonic decays, such as $B^+ \to p\overline{p}\mu^+\nu_\mu$, where such final-state interactions are absent.

In this paper, the first observation of the decay $B^+ \to p\overline{p}\mu^+\nu_\mu$ is presented. As the dynamics of the transition are not known, the branching fraction is measured in bins of $p\overline{p}$ invariant mass. These bins are then summed to obtain a measurement of the total branching fraction. The decay $B^+ \to J/\psi\, K^+$, with $J/\psi \to \mu^+\mu^-$ is chosen as the normalisation mode as it is fully reconstructed and can pass similar selection requirements to the signal. The branching fraction within a bin i is

$$\mathcal{B}_i(B^+ \to p\overline{p}\mu^+\nu_\mu) = \frac{N_i(B^+ \to p\overline{p}\mu^+\nu_\mu)}{N(B^+ \to (J/\psi \to \mu^+\mu^-)K^+)} \times \frac{\epsilon(B^+ \to (J/\psi \to \mu^+\mu^-)K^+)}{\epsilon_i(B^+ \to p\overline{p}\mu^+\nu_\mu)} \times \mathcal{B}(B^+ \to (J/\psi \to \mu^+\mu^-)K^+), \quad (1)$$

where $N_i(B^+ \to p\overline{p}\mu^+\nu_\mu)$ is the yield of $B^+ \to p\overline{p}\mu^+\nu_\mu$ candidates in bin i, $N(B^+ \to (J/\psi \to \mu^+\mu^-)K^+)$ is the total yield of $B^+ \to J/\psi\, K^+$ candidates and ϵ represents the product of the detector acceptance and the reconstruction and selection

efficiencies of the two modes. The branching fractions of $B^+ \to J/\psi\, K^+$ and $J/\psi \to \mu^+\mu^-$ decays are taken from Ref. [12].

The signal yields are extracted from fits to a variable called the corrected mass, which accounts for the unreconstructed neutrino in the signal decay. It is defined by [18]

$$m_{\rm corr} = |p'_{\rm T}| + \sqrt{|p'_{\rm T}|^2 + m^2_{\rm vis}}, \tag{2}$$

where $|p'_{\rm T}|$ is defined as the magnitude of the reconstructed $p\overline{p}\mu^+$ momentum transverse to the B flight direction and $m^2_{\rm vis}$ as the square of the $p\overline{p}\mu^+$ invariant mass.

This study uses the data collected with the LHCb detector in proton-proton collisions in 2011, 2012 and 2016. This corresponds to integrated luminosities of 1.0, 2.0 and 1.9 fb^{-1} at centre-of-mass energies of 7, 8 and 13 TeV, respectively. The 2011 and 2012 data sets are treated together and collectively referred as the Run 1 data set. Charge conjugate processes are implied throughout this paper.

2 Detector and simulation

The LHCb detector [19, 20] is a single-arm forward spectrometer covering the pseudorapidity range $2 < \eta < 5$, designed for the study of particles containing b or c quarks. The detector includes a high-precision tracking system consisting of a silicon-strip vertex detector surrounding the pp interaction region [21], a large-area silicon-strip detector located upstream of a dipole magnet with a bending power of about 4 Tm, and three stations of silicon-strip detectors and straw drift tubes [22, 23] placed downstream of the magnet. The tracking system provides a measurement of the momentum, p, of charged particles with a relative uncertainty that varies from 0.5% at low momentum to 1.0% at 200 GeV/c. The minimum distance of a track to a primary vertex (PV), the impact parameter (IP), is measured with a resolution of $(15 + 29/p_{\rm T})\,\mu$m, where $p_{\rm T}$ is the component of the momentum transverse to the beam in GeV/c. Different types of charged hadrons are distinguished using information from two ring-imaging Cherenkov (RICH) detectors [24]. Photons, electrons and hadrons are identified by a calorimeter system consisting of scintillating-pad and preshower detectors, an electromagnetic and a hadronic calorimeter. Muons are identified by a system composed of alternating layers of iron and multiwire proportional chambers [25].

The online event selection is performed by a trigger [26], which consists of a hardware stage that performs some basic selection, followed by a software stage, which applies a full event reconstruction. At the first level, a track consistent with being a muon with significant $p_{\rm T}$ is required to be present in the event. Subsequently in the software stage, two tracks are required to form a secondary vertex with significant displacement from a pp interaction vertex. A multivariate algorithm [27] is used to identify vertices that are consistent with the decay of a b hadron.

Simulation is used to determine the efficiency of the signal mode and estimate the shapes of the signal and several backgrounds modes in the fits to the $m_{\rm corr}$ distribution. In the simulation, pp collisions are generated using Pythia [28] with a specific LHCb configuration [29]. Decays of unstable particles are described by EvtGen [30], in which final-state radiation is generated using Photos [31]. The interaction of the generated particles with the detector, and its response, are implemented using the Geant4 toolkit [32],

as described in Ref. [33]. The generated B meson p and $p_{\rm T}$ spectra are corrected to match the data distributions. A boosted decision tree (BDT) reweighter [34] is trained on samples of $B^+ \to J/\psi\, K^+$ data and simulation, independent of those used for the normalisation of the branching fraction. This is then used to correct all the simulation samples used in the analysis.

3 Selection

Signal candidates are constructed from three charged tracks which are required to be of good quality and have a large IP with respect to any PV. The tracks must also have particle identification criteria consistent with their particle hypothesis. The requirement for positive proton identification in turn enforces a minimum value of p of $18\,{\rm GeV}/c$ such that they are above the threshold for radiating in the RICH. Similarly, the muons must have p above $3\,{\rm GeV}/c$ to propagate through the muon stations. All the tracks must have $p_{\rm T}$ larger than $1.5\,{\rm GeV}/c$ and form a good quality vertex significantly displaced from the PV with which the candidate is associated. The signal muon must have fired the hardware trigger and the reconstructed B^+ candidate formed by the three tracks must be consistent with the object that fired the software trigger. Potential decays of η_c, J/ψ and $\psi(2S)$ mesons to $p\overline{p}$ are vetoed with cuts on the $p\overline{p}$ invariant mass of $\pm 50\,{\rm MeV}/c^2$ around their respective known masses [12].

The selection of the $B^+ \to (J/\psi \to \mu^+\mu^-)K^+$ normalisation mode is aligned with that of the signal to reduce systematic uncertainties. The cuts on the signal protons are applied to the kaon and the muon of opposite sign ($K^+\mu^-$), with the exception of the particle identification criteria. The selection of the other muon is the same as that of the muon in the signal decay.

Further selection is used to reduce several sources of backgrounds relative to the signal. In total there are five variables to which selection is applied, with the chosen cuts on each optimised together. These variables, and the backgrounds targeted by them are described in the following paragraphs.

The largest background contribution comes from a melange of partially reconstructed decays producing two protons and a muon in the final state. It is expected that the largest among these originates in $b \to c$ quark transitions. The most pernicious is $B \to \overline{\Lambda}_c^- p\mu^+\nu_\mu X$ decays, where X represents any number of charged or neutral pions (including none) and the $\overline{\Lambda}_c^-$ decays to a final state including one proton. The other major background arises from $B \to p\overline{p}DX$ decays, where the D meson may be of any variety (D^0, D^+, D^{*+}, *etc.*) and ultimately decays to a final state with a muon. The contribution of $B \to p\overline{\Lambda}_c^- X$ decays with the $\overline{\Lambda}_c^-$ decaying semileptonically is comparatively small, as the semileptonic branching fraction is dominated by $\overline{\Lambda}_c^- \to \Lambda l^- \bar{\nu}_l$ decays. The Λ baryon flies a sufficient distance within the detector before decaying such that the resulting proton is not associated with the B decay vertex. Another source of partially reconstructed background is formed of $B \to p\overline{p}\mu^+\nu_\mu X$ decays, where X denotes one or more charged or neutral pions. These decays may proceed with intermediate N^* or Δ resonances and could naively be expected to have similar branching fractions to the signal.

If any of these partially reconstructed decay modes produces more than three charged tracks, it can be efficiently dealt with by an isolation technique. Once a signal candidate has been constructed, the other tracks in the event close to the B decay vertex are

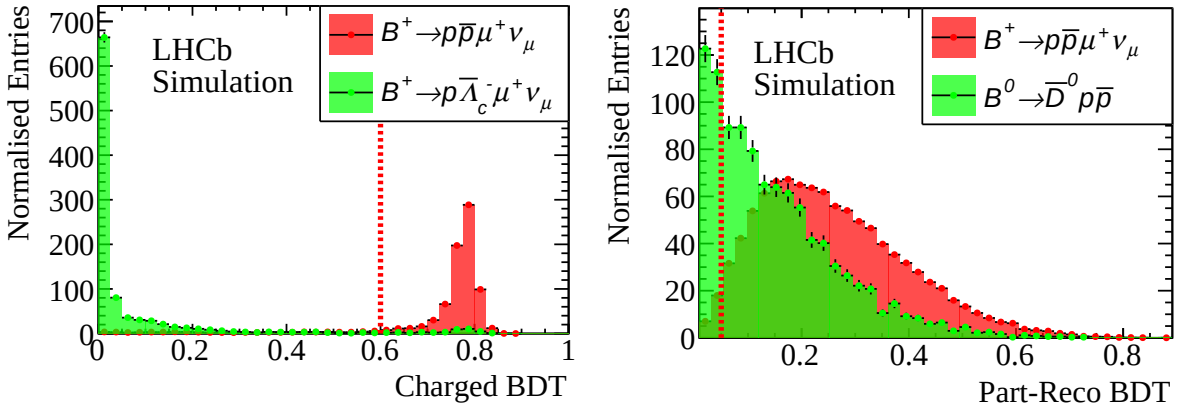

Figure 1: The result of training the (left) charged-isolation BDT and the (right) part-reco BDT. The chosen cut values are indicated by the red line. For some events there are no additional tracks near the B-decay vertex; these events are accepted and do not appear in the charged BDT output. The background samples shown here have the Λ_c^+ and $\overline{D}^0$ decaying via $\Lambda_c^+ \to pK^+\pi^-$ and $\overline{D}^0 \to \mu^+ X$. The part-reco BDT is trained on a mixture of background modes with only one shown here for illustration.

examined. A BDT is used to identify those nearby tracks that can be associated with the signal candidate decay-vertex. If the candidate is truly signal, there should be few other tracks that can be associated with it and the BDT should classify them with a low score. On the other hand, the extra track(s) from a partially reconstructed decay will give a high score if such tracks are found. The isolation algorithm returns the BDT output for the four tracks most likely to have come from the B vertex. These four numbers are themselves combined into a single BDT classifier, known as the charged-isolation BDT. This BDT is trained on simulation to discriminate signal from $B^+ \to \overline{\Lambda}_c^- p\mu^+\nu_\mu$, which is expected to be the largest decay mode with extra charged tracks. The efficacy of this BDT in reducing such background is shown in Fig. 1. On its own, the indicated cut point on the charged BDT score rejects 80% of the major background decay $B \to \overline{\Lambda}_c^- p\mu^+\nu_\mu X$, whilst retaining 93% of the signal.

For those partially reconstructed final states with only additional neutral particles, further suppression is achieved by considering the kinematics of the decays. An additional BDT, the so called part-reco BDT, considers 11 variables: the impact parameter significance of the three final-state tracks, the $p\overline{p}$ pair and the B^+ candidate with respect to the PV; the impact parameters of the tracks with respect to the fitted B^+ decay vertex; the χ^2 of the B^+ vertex fit; the angle between the B^+ candidate momentum and displacement vectors; and the difference between the p and $\overline{p}$ momenta. The part-reco BDT is trained on simulation in order to discriminate signal from a mixture of all the considered background modes. The result of this training is shown in Fig. 1. The selection on the part-reco BDT output removes 18% of the decays $B \to p\overline{p}D$ and keeps 98% of the signal.

An additional background arises from particles that are misidentified as protons (misID). The particle identification requirements on the proton tracks are therefore further tightened. The background due to the muon being another misidentified particle is considered and is reduced to a negligible amount with only a loose particle identification requirement.

In addition to the two BDTs and proton identification criteria, one further quantity

is considered. The uncertainty on the corrected mass of the candidate is powerful in improving the separation between signal and background [35]. It is calculated from the estimated uncertainties on the positions of the B^+ primary and secondary vertices, and the momenta of the tracks. Selecting lower values of the corrected-mass uncertainty produces a sharper peak for the signal mode in the corrected mass distribution, which will aid the discrimination of the signal from background in the fit to determine the yield. Therefore, in total the selection uses five quantities (two BDTs, the proton PID, the muon PID and the corrected-mass uncertainty). In order to ascertain the optimal cut point, a five dimensional grid search is performed using pseudoexperiments. Data sets are generated from the simulation samples with the expected proportions of each background. The expected signal amount is taken from the central value of the $B^+ \to p\overline{p}e^+\nu_e$ branching fraction reported by the Belle collaboration [11]. For the backgrounds, the current averages for the branching fractions are used if they have been measured. For those backgrounds that have not been measured, their branching fractions are estimated relative to that expected for the signal, accounting for different CKM matrix elements and the available phase space. For each set of cuts in the grid, the selection is applied to the simulation to estimate the efficiency for each component. The efficiency of the PID cuts on the simulation is estimated with a method based on data control samples [36]. For each data set the $m_{\rm corr}$ variable is generated and the expected relative uncertainty on the signal yield is found by a fit to the simulated data. These fits are not binned in $m(p\overline{p})$ but consider the entire sample as a whole. The set of cuts that produces the smallest relative uncertainty on the signal yield is chosen.

4 Signal and normalisation yields

The yields of the signal and normalisation modes are ascertained with unbinned extended maximum-likelihood fits. In the case of the normalisation mode, the invariant mass distribution of the $J/\psi K^+$ candidates is fitted. The 2011, 2012 and 2016 data sets are fitted separately and then the yields combined. These fits are shown in Fig. 2.

For the signal mode, the corrected mass is fitted. The distribution of this variable peaks at the known B^+ rest mass for candidates where one massless particle is not reconstructed. On the other hand, candidates from partially reconstructed decays that are missing one or more massive particles in addition to the neutrino have wide distributions concentrated at lower corrected mass values. The Run 1 and 2016 data are combined and fitted together to improve the fit stability.

The shapes for the signal component and contributions from partially reconstructed decays are determined using simulation. The shape of the signal probability density function (PDF) is parametrised by the sum of four bifurcated Gaussian functions with a common mean. The parameters of the Gaussian functions as well as their relative fractions are all fixed in the fit. All of the background PDFs are accounted for with kernel density estimation [37]. The shape of the proton misID background comes from a separate independent data sample in which the particle identification requirements on one of the protons have been removed. Using this data sample, the expected number of proton misID candidates can be estimated and used as a constraint in the fit. A background component due to random combinations of protons and muons, referred to as the combinatorial background, is included in the fit. A sample of data for which the B^+ decay vertex quality

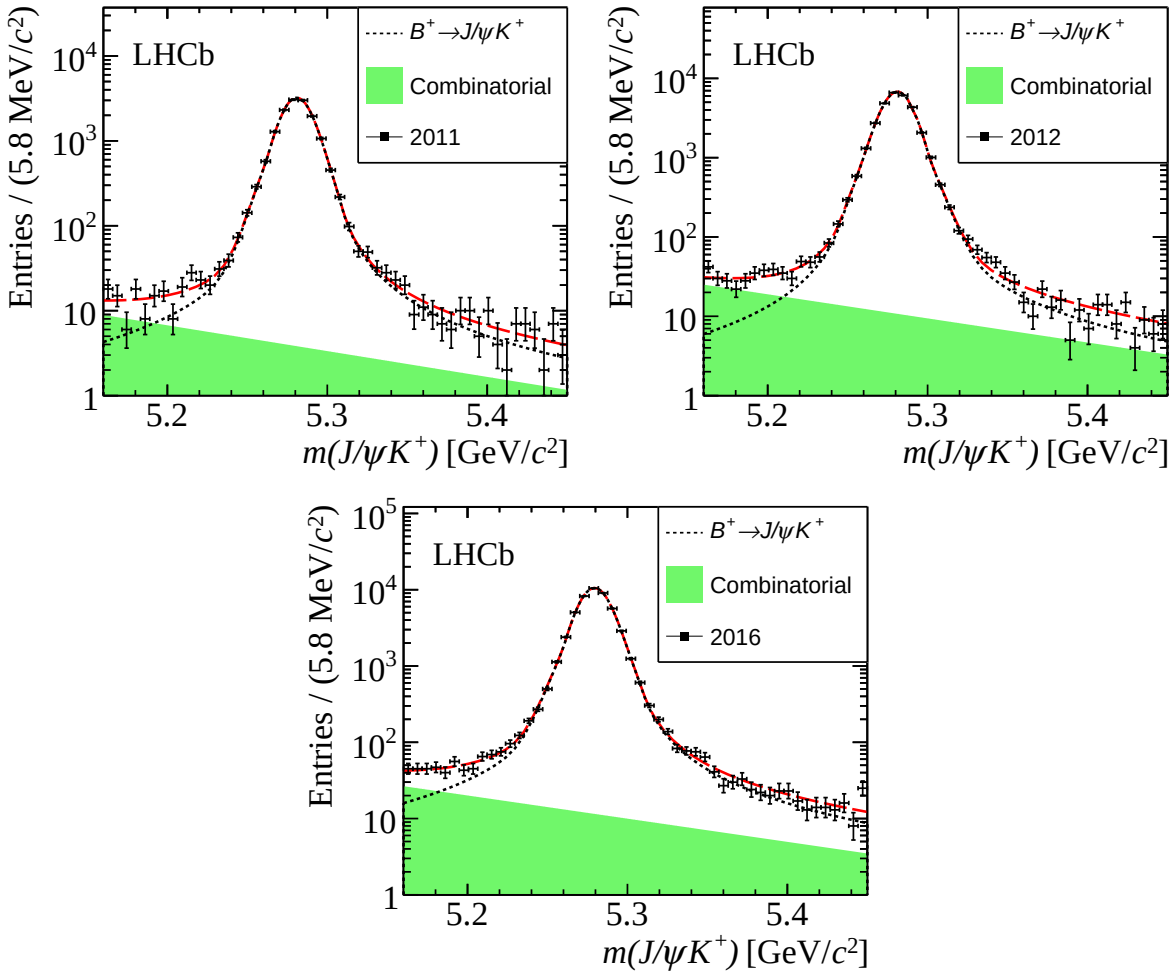

Figure 2: Distribution of $m(J/\psi\, K^+)$ with the fit result shown for the (top left) 2011 data, (top right) 2012 and (bottom) 2016.

selection has been reversed is used to estimate the shape of this background.

The yields of the signal, proton misID, combinatorial and partially reconstructed decays are determined by the fit, as are the relative fractions of each partially reconstructed mode. All of the fit parameters are free with the exception of the misID yield which is constrained.

The fit in each $m(p\overline{p})$ bin is performed independently. The $m_{\rm corr}$ distributions in each bin, and the resulting fits are shown in Fig. 3. In each bin the fits are validated using pseudoexperiments. An ensemble of 10^5 data sets is generated and fitted with the component yields taken from the fits to data. Some small biases on the signal yield are found and these are considered as a source of systematic uncertainty.

5 Efficiency

The efficiencies for the signal and normalisation modes to be reconstructed and selected are both assessed with simulation. Corrections are applied to account for known differences between data and simulation in the track-reconstruction efficiency [38] and the efficiency

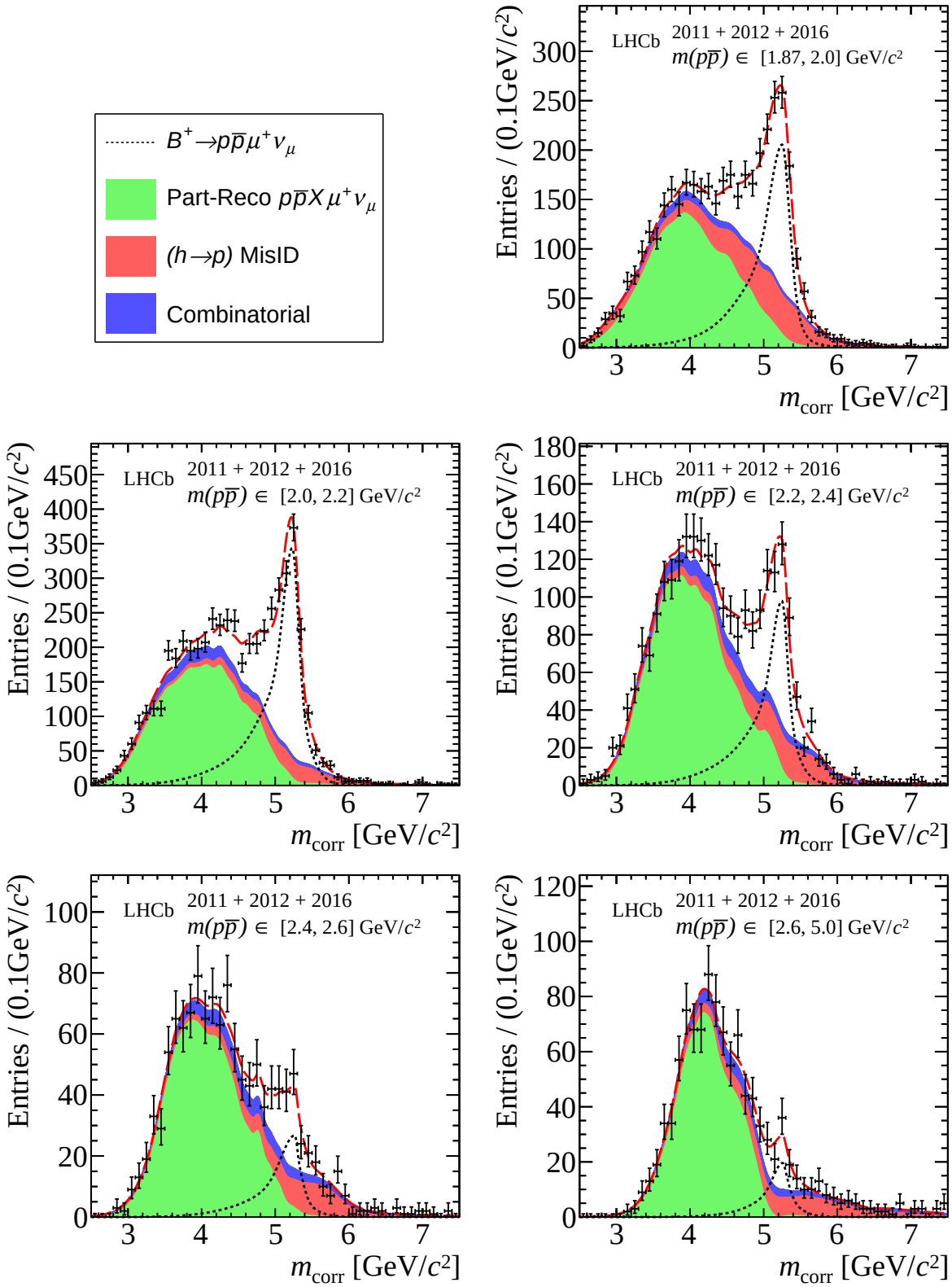

Figure 3: Distributions of $m_{\rm corr}$ in each $m(p\bar{p})$ bin with the fit results shown.

Table 1: The relative efficiencies for Run 1 and 2016 and the weighted combination of both.

$m(p\overline{p})_i$ [GeV/c^2]	$\epsilon(B \to p\overline{p}\mu\nu)_i/\epsilon(B \to J/\psi K)$		
	Run 1	2016	Run 1 & 2016
Bin 1: $1.87 - 2.0$	0.37 ± 0.02	0.57 ± 0.03	0.48 ± 0.02
Bin 2: $2.0 - 2.2$	0.37 ± 0.02	0.51 ± 0.03	0.45 ± 0.02
Bin 3: $2.2 - 2.4$	0.36 ± 0.02	0.50 ± 0.03	0.44 ± 0.02
Bin 4: $2.4 - 2.6$	0.36 ± 0.02	0.52 ± 0.03	0.45 ± 0.02
Bin 5: $2.6 - 5.0$	0.35 ± 0.02	0.49 ± 0.02	0.43 ± 0.02

of the hardware trigger [39]. The efficiency of the particle identification requirements on each track is evaluated with data [36] and applied to the simulation.

The binning in $m(p\overline{p})$ reduces the dependence on the model of the B^+ decay when calculating the efficiency of the signal mode. However, as the selection cuts on kinematic quantities of the candidates, there is still some residual dependence on the dynamics of the decay. The simulation is therefore weighted to represent the pQCD model of Ref. [8] as the current best estimate of how the decay proceeds. This weighting corrects the distribution of the invariant mass of the $\mu^+\nu_\mu$ system. The variation of the parameters of this model is considered as a source of systematic uncertainty.

The ratio of selection efficiencies between the signal and normalisation modes in each bin of $m(p\overline{p})$ is shown in Table 1. These efficiencies are presented separately for the Run 1 and 2016 samples. They are combined to form an overall efficiency ratio, accounting for the difference in sample sizes between Run 1 and 2016. This combination is calculated using the measured B^+ production cross-sections [40] and integrated luminosities of each data set.

6 Systematic uncertainties

The systematic uncertainties can be split into two categories: those that affect the calculation of the ratio of efficiencies of the signal and normalisation modes and those that may change the determination of the signal yield in the fit. For the former, each of the corrections to the simulation contributes a source of uncertainty both from the limited sizes of the samples used to derive the corrections and from the method of deriving them. The parameters of the BDT reweighter used to correct the distributions of p and $p_{\rm T}$ of the B^+ are altered and the relative efficiencies recalculated. An additional uncertainty due to any residual differences between data and simulation is determined using the $B^+ \to J/\psi K^+$ decay mode. The difference in efficiency when cutting on the two BDTs and corrected-mass uncertainty is compared between data and simulation for the mode.

To account for the uncertainty in the correction of the simulation for the reconstruction efficiency of each track, the applied weights are varied within their uncertainties and the relative efficiencies recalculated. Similarly, an uncertainty is assessed for the particle identification weights applied to each track. The uncertainty due to the limited simulation sample sizes used to calculate the efficiencies is also included.

A further uncertainty is due to the physics model that the simulation is weighted to represent. The model affects the kinematic distributions of the daughter tracks which

feeds into the efficiency calculation as these distributions are cut on. Due to the model being unproven, a conservative uncertainty is taken. New sets of weights for the simulation are created that sample extreme variations of the model parameters ($\pm 5\,\sigma$), and for each variation the efficiency is recalculated. Despite this extreme test, the systematic due to the physics model is not dominant, which reflects the flat selection efficiency over the kinematic ranges in which the final-state particles lie within each bin of $m(p\overline{p})$. Finally, the uncertainties on the B^+ production cross-section [40] and integrated luminosities of the data samples are combined to give the systematic uncertainty on the averaging of the efficiencies when combining Run 1 and 2016.

In the corrected-mass fit, uncertainties arise from potential variations in the shapes of the components. This variation is assessed with pseudoexperiments. Data sets are generated with the nominal fit model and then fitted with both the nominal model and an alternative. The width of the distribution of differences between the nominal and alternative fits gives the uncertainty. For those components that rely on kernel density estimators, a systematic is assessed for the choice of smoothing parameter by varying it. The uncertainty due to the choice of model for the signal shape is found by replacing the nominal PDF with one constructed with kernel density estimators. The uncertainty due to the limited sizes of the simulation samples is determined by generating new simulation from the nominal fit PDFs with the same statistics and making alternative PDFs with those samples. Similarly, an estimate of the uncertainty on the shape of the proton misID background component is assessed. For the shape of the combinatorial background component, an alternative data sample is trialled which requires the two protons to be of the same charge. Finally, the small biases in the fit noted in Sec. 4 are included.

A summary of the systematic uncertainties is presented in Table 2. They are given as relative uncertainties on the branching fraction with the combination accounting for the correlation of the uncertainties between the two data sets. The correlations of the total uncertainties between the bins is shown in Fig. 5 and the covariance matrix is presented in Table 4, both in the appendix.

7 Results

The fitted yields for the signal mode are presented in Table 3. The extracted yields of the normalisation channel are $14\,930 \pm 260$ for 2011, $31\,380 \pm 190$ for 2012 and $49\,270 \pm 250$ for 2016. Combining these with the efficiency ratios from Sec. 5, the differential branching fraction in each $m(p\overline{p})$ bin is calculated relative to the branching fraction of the normalisation mode. The results are presented in Table 3. The relative differential branching fractions are summed over the bins, with the correlation of the systematic uncertainties between the bins accounted for, to give the total relative branching fraction of

$$\frac{\mathcal{B}(B^+ \to p\overline{p}\mu^+\nu_\mu)}{\mathcal{B}(B^+ \to (J/\psi \to \mu^+\mu^-)K^+)} = (8.75 \pm 0.39 \pm 0.35) \times 10^{-2},$$

where the first uncertainty is statistical and the second systematic. Multiplying this by the current average of the normalisation branching fraction [12] leads to

$$\mathcal{B}(B^+ \to p\overline{p}\mu^+\nu_\mu) = (5.27^{+0.23}_{-0.24} \pm 0.21 \pm 0.15) \times 10^{-6},$$

where the third uncertainty is from the normalisation branching fraction. Finally, the absolute differential branching fraction as a function of $m(p\overline{p})$ is shown in Fig. 4, where

Table 2: A summary of the systematic uncertainties on the differential branching fractions. The contributions pertaining to the efficiency estimate are first, those for the yield extraction are below. The particle identification and tracking efficiency uncertainties are assumed to be 100% correlated between Run 1 and 2016. The total correlations of the uncertainties between the bins is shown in Fig. 5.

Source	Relative uncertainties on $\mathcal{B}$ [%]				
	Bin 1	Bin 2	Bin 3	Bin 4	Bin 5
Kinematic reweighting	0.7	0.6	0.4	0.5	0.4
Data-simulation agreement	0.4	0.4	0.4	0.4	0.4
Tracking efficiency	2.7	2.7	2.7	2.7	2.7
Particle identification	1.0	0.7	1.3	1.0	1.7
Simulation sample size	3.6	3.2	3.2	3.1	3.0
Physics model	0.3	0.6	0.6	0.4	0.3
Run 1 and 2016 combination	2.1	1.6	1.7	1.7	1.6
Kernel smoothing	0.0	1.1	2.7	7.9	3.5
Signal model	0.6	2.0	3.0	4.8	9.9
Simulation sample size	0.3	0.0	0.3	2.4	5.2
misID model	0.9	0.1	0.6	5.2	13.5
Combinatorial model	0.9	1.2	1.2	8.5	4.7
Fit bias	0.2	0.1	0.9	2.5	7.8
Total systematic uncertainty	5.3	5.2	6.5	15.6	20.8
Total statistical uncertainty	9.1	5.5	12.5	25.3	29.8

the indicated uncertainties include statistical, systematic and normalisation uncertainty contributions. As expected from the theory model and the analogous hadronic decays, the differential distribution peaks at a very low value and falls off sharply. The measured total branching fraction agrees with the previous measurement from the Belle collaboration and represents the first observation of the $B^+ \to p\bar{p}\mu^+\nu_\mu$ decay mode.

Table 3: Number of observed $B^+ \to p\bar{p}\mu^+\nu_\mu$ candidates and differential branching fraction in each bin of $m(p\bar{p})$. In the centre column the uncertainties are statistical only. In the right the first uncertainties are statistical, the second systematic and the third from the normalisation branching fractions.

$m(p\bar{p})$ [GeV/c^2]	Signal Yield	$d\mathcal{B}(B^+ \to p\bar{p}\mu^+\nu_\mu)/dm(p\bar{p})$ [$\times 10^{-6}$ GeV^{-1}c^2]
Bin 1: $1.87 - 2.0$	1208^{+110}_{-110}	$12.86^{+1.18}_{-1.17} \pm 0.69 \pm 0.38$
Bin 2: $2.0 - 2.2$	1826^{+97}_{-110}	$12.88^{+0.69}_{-0.74} \pm 0.68 \pm 0.38$
Bin 3: $2.2 - 2.4$	526^{+67}_{-64}	$3.78^{+0.48}_{-0.46} \pm 0.24 \pm 0.11$
Bin 4: $2.4 - 2.6$	148^{+40}_{-35}	$1.04^{+0.28}_{-0.25} \pm 0.16 \pm 0.03$
Bin 5: $2.6 - 5.0$	88^{+26}_{-26}	$0.054^{+0.016}_{-0.016} \pm 0.011 \pm 0.002$

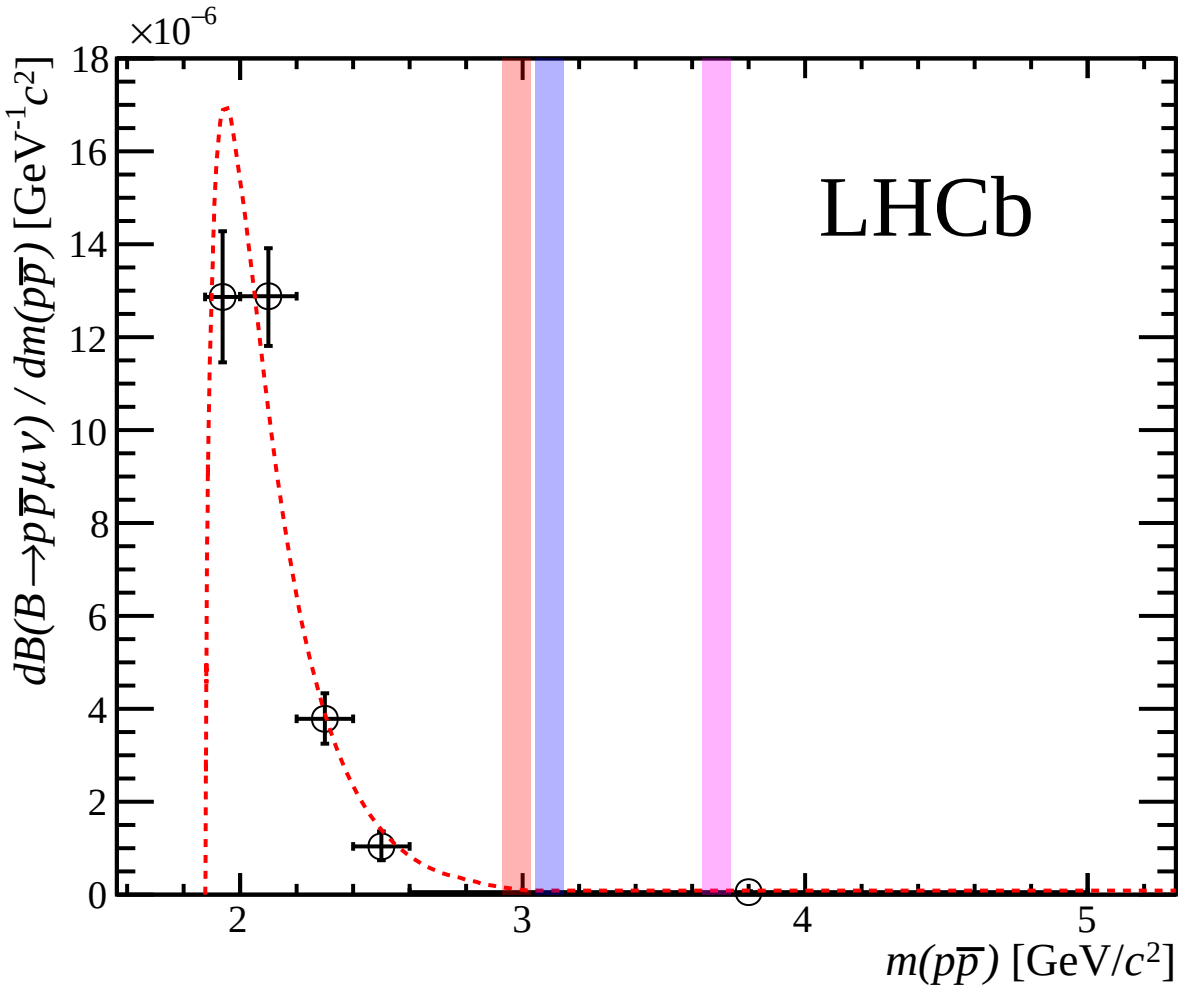

Figure 4: Differential branching fraction as a function of the $p\bar{p}$ invariant mass. The $\eta_c \to p\bar{p}$, $J/\psi \to p\bar{p}$ and $\psi(2S) \to p\bar{p}$ vetoes are indicated by the (left) red, (middle) blue and (right) pink bands, respectively. The red dashed line represents the prediction of the pQCD model normalised to the observed branching fraction [8].

Acknowledgements

We express our gratitude to our colleagues in the CERN accelerator departments for the excellent performance of the LHC. We thank the technical and administrative staff at the LHCb institutes. We acknowledge support from CERN and from the national agencies: CAPES, CNPq, FAPERJ and FINEP (Brazil); MOST and NSFC (China); CNRS/IN2P3 (France); BMBF, DFG and MPG (Germany); INFN (Italy); NWO (Netherlands); MNiSW and NCN (Poland); MEN/IFA (Romania); MSHE (Russia); MinECo (Spain); SNSF and SER (Switzerland); NASU (Ukraine); STFC (United Kingdom); DOE NP and NSF (USA). We acknowledge the computing resources that are provided by CERN, IN2P3 (France), KIT and DESY (Germany), INFN (Italy), SURF (Netherlands), PIC (Spain), GridPP (United Kingdom), RRCKI and Yandex LLC (Russia), CSCS (Switzerland), IFIN-HH (Romania), CBPF (Brazil), PL-GRID (Poland) and OSC (USA). We are indebted to the communities behind the multiple open-source software packages on which we depend. Individual groups or members have received support from AvH Foundation (Germany);

EPLANET, Marie Skłodowska-Curie Actions and ERC (European Union); ANR, Labex P2IO and OCEVU, and Région Auvergne-Rhône-Alpes (France); Key Research Program of Frontier Sciences of CAS, CAS PIFI, and the Thousand Talents Program (China); RFBR, RSF and Yandex LLC (Russia); GVA, XuntaGal and GENCAT (Spain); the Royal Society and the Leverhulme Trust (United Kingdom).

8 Appendix

Figure 5: The correlations in the uncertainties between bins of $p\overline{p}$ mass.

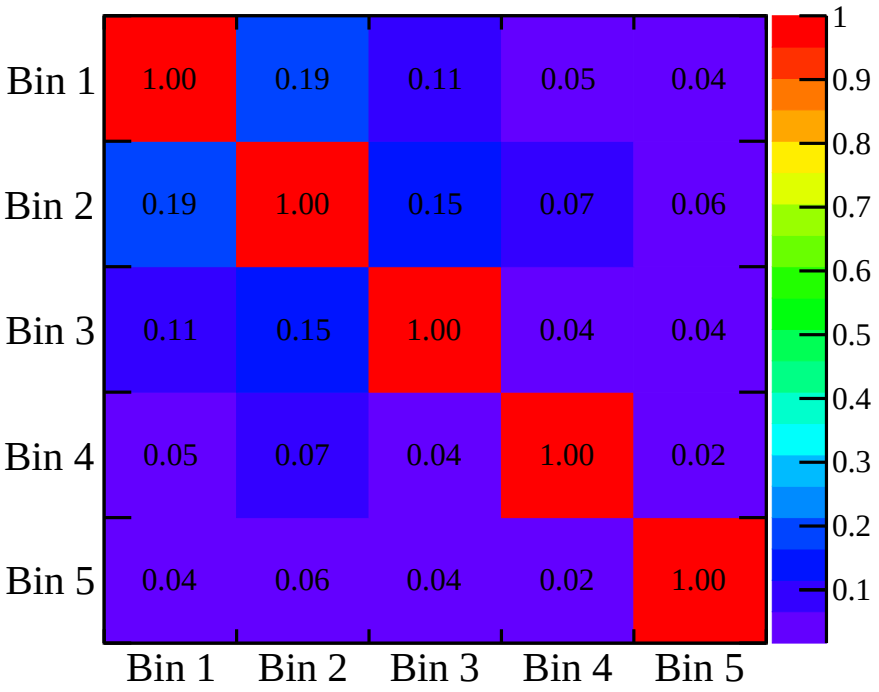

Table 4: The covariance matrix for bins of $m(p\overline{p})$.

	Bin 1	Bin 2	Bin 3	Bin 4	Bin 5
$m(p\overline{p})$ [GeV/c^2]	$1.87-2.0$	$2.0-2.2$	$2.2-2.4$	$2.4-2.6$	$2.6-5.0$
$1.87-2.0$	2.0×10^{-12}	2.8×10^{-13}	8.5×10^{-14}	2.3×10^{-14}	1.2×10^{-15}
$2.0-2.2$	2.8×10^{-13}	1.1×10^{-12}	8.3×10^{-14}	2.3×10^{-14}	1.2×10^{-15}
$2.2-2.4$	8.5×10^{-14}	8.3×10^{-14}	2.9×10^{-13}	6.9×10^{-15}	3.8×10^{-16}
$2.4-2.6$	2.3×10^{-14}	2.3×10^{-14}	6.9×10^{-15}	9.6×10^{-14}	1.0×10^{-16}
$2.6-5.0$	1.2×10^{-15}	1.2×10^{-15}	3.8×10^{-16}	1.0×10^{-16}	3.9×10^{-16}

References

[1] LHCb collaboration, R. Aaij *et al.*, *Measurement of the ratio of the $\mathcal{B}(B^0 \to D^{*-}\tau^+\nu_\tau)$ and $\mathcal{B}(B^0 \to D^{*-}\mu^+\nu_\mu)$ branching fractions using three-prong τ-lepton decays*, Phys. Rev. Lett. **120** (2018) 171802, arXiv:1708.08856.

[2] LHCb collaboration, R. Aaij *et al.*, *Measurement of the ratio of branching fractions $\mathcal{B}(\overline{B}^0 \to D^{*+}\tau^-\overline{\nu}_\tau)/\mathcal{B}(\overline{B}^0 \to D^{*+}\mu^-\overline{\nu}_\mu)$*, Phys. Rev. Lett. **115** (2015) 111803, Publisher's Note ibid. **115** (2015) 159901, arXiv:1506.08614.

[3] Belle collaboration, A. Abdesselam *et al.*, *Measurement of $\mathcal{R}(D)$ and $\mathcal{R}(D^*)$ with a semileptonic tagging method*, arXiv:1904.08794.

[4] Belle collaboration, S. Hirose *et al.*, *Measurement of the τ lepton polarization and $R(D^*)$ in the decay $\bar{B} \to D^*\tau^-\bar{\nu}_\tau$*, Phys. Rev. Lett. **118** (2017) 211801, arXiv:1612.00529.

[5] Belle collaboration, M. Huschle *et al.*, *Measurement of the branching ratio of $\bar{B} \to D^{(*)}\tau^-\bar{\nu}_\tau$ relative to $\bar{B} \to D^{(*)}\ell^-\bar{\nu}_\ell$ decays with hadronic tagging at Belle*, Phys. Rev. **D92** (2015) 072014, arXiv:1507.03233.

[6] BaBar collaboration, J. P. Lees *et al.*, *Evidence for an excess of $\bar{B} \to D^{(*)}\tau^-\bar{\nu}_\tau$ decays*, Phys. Rev. Lett. **109** (2012) 101802, arXiv:1205.5442.

[7] Heavy Flavor Averaging Group, Y. Amhis *et al.*, *Averages of b-hadron, c-hadron, and τ-lepton properties as of summer 2016*, Eur. Phys. J. **C77** (2017) 895, arXiv:1612.07233, updated results and plots available at https://hflav.web.cern.ch.

[8] C. Q. Geng and Y. K. Hsiao, *Semileptonic $B^- \to p\bar{p}\ell^-\bar{\nu}_\ell$ decays*, Phys. Lett. **B704** (2011) 495, arXiv:1107.0801.

[9] C. Q. Geng and Y. K. Hsiao, *Angular distributions in three-body baryonic b decays*, Phys. Rev. D **74** (2006) 094023.

[10] C.-H. Chen, H.-Y. Cheng, C. Q. Geng, and Y. K. Hsiao, *Charmful three-body baryonic b decays*, Phys. Rev. D **78** (2008) 054016.

[11] Belle collaboration, K.-J. Tien *et al.*, *Evidence for semileptonic $B^- \to p\bar{p}l^-\bar{\nu}_l$ decays*, Phys. Rev. **D89** (2014) 011101, arXiv:1306.3353.

[12] Particle Data Group, M. Tanabashi *et al.*, *Review of particle physics*, Phys. Rev. **D98** (2018) 030001.

[13] LHCb collaboration, R. Aaij *et al.*, *First observation of the rare purely baryonic decay $B^0 \to p\overline{p}$*, Phys. Rev. Lett. **119** (2017) 232001, arXiv:1709.01156.

[14] BaBar collaboration, B. Aubert *et al.*, *Evidence for the $B^0 \to p\bar{p}K^{*0}$ and $B^+ \to \eta_c K^{*+}$ decays and study of the decay dynamics of B meson decays into $p\bar{p}h$ final states*, Phys. Rev. **D76** (2007) 092004, arXiv:0707.1648.

[15] BaBar collaboration, B. Aubert *et al.*, *Measurements of the decays $B^0 \to \bar{D}^0 p\bar{p}$, $B^0 \to \bar{D}^{*0} p\bar{p}$, $B^0 \to D^- p\bar{p}\pi^+$, and $B^0 \to D^{*-} p\bar{p}\pi^+$*, Phys. Rev. **D74** (2006) 051101, arXiv:hep-ex/0607039.

[16] Belle collaboration, M. Z. Wang *et al.*, *Observation of $B^+ \to p\bar{p}\pi^+$, $B^0 \to p\bar{p}K^0$, and $B^+ \to p\bar{p}K^{*+}$*, Phys. Rev. Lett. **92** (2004) 131801, arXiv:hep-ex/0310018.

[17] LHCb collaboration, R. Aaij *et al.*, *Evidence for CP violation in $B^+ \to p\bar{p}K^+$ Decays*, Phys. Rev. Lett. **113** (2014) 141801, arXiv:1407.5907.

[18] SLD collaboration, K. Abe *et al.*, *A Measurement of R_b using a vertex mass tag*, Phys. Rev. Lett. **80** (1998) 660, arXiv:hep-ex/9708015.

[19] LHCb collaboration, A. A. Alves Jr. *et al.*, *The LHCb detector at the LHC*, JINST **3** (2008) S08005.

[20] LHCb collaboration, R. Aaij *et al.*, *LHCb detector performance*, Int. J. Mod. Phys. **A30** (2015) 1530022, arXiv:1412.6352.

[21] R. Aaij *et al.*, *Performance of the LHCb Vertex Locator*, JINST **9** (2014) P09007, arXiv:1405.7808.

[22] R. Arink *et al.*, *Performance of the LHCb Outer Tracker*, JINST **9** (2014) P01002, arXiv:1311.3893.

[23] P. d'Argent *et al.*, *Improved performance of the LHCb Outer Tracker in LHC Run 2*, JINST **12** (2017) P11016, arXiv:1708.00819.

[24] M. Adinolfi *et al.*, *Performance of the LHCb RICH detector at the LHC*, Eur. Phys. J. **C73** (2013) 2431, arXiv:1211.6759.

[25] A. A. Alves Jr. *et al.*, *Performance of the LHCb muon system*, JINST **8** (2013) P02022, arXiv:1211.1346.

[26] R. Aaij *et al.*, *The LHCb trigger and its performance in 2011*, JINST **8** (2013) P04022, arXiv:1211.3055.

[27] V. V. Gligorov and M. Williams, *Efficient, reliable and fast high-level triggering using a bonsai boosted decision tree*, JINST **8** (2013) P02013, arXiv:1210.6861.

[28] T. Sjöstrand, S. Mrenna, and P. Skands, *PYTHIA 6.4 physics and manual*, JHEP **05** (2006) 026, arXiv:hep-ph/0603175; T. Sjöstrand, S. Mrenna, and P. Skands, *A brief introduction to PYTHIA 8.1*, Comput. Phys. Commun. **178** (2008) 852, arXiv:0710.3820.

[29] I. Belyaev *et al.*, *Handling of the generation of primary events in Gauss, the LHCb simulation framework*, J. Phys. Conf. Ser. **331** (2011) 032047.

[30] D. J. Lange, *The EvtGen particle decay simulation package*, Nucl. Instrum. Meth. **A462** (2001) 152.

[31] P. Golonka and Z. Was, *PHOTOS Monte Carlo: A precision tool for QED corrections in Z and W decays*, Eur. Phys. J. **C45** (2006) 97, arXiv:hep-ph/0506026.

[32] Geant4 collaboration, J. Allison *et al.*, *Geant4 developments and applications*, IEEE Trans. Nucl. Sci. **53** (2006) 270; Geant4 collaboration, S. Agostinelli *et al.*, *Geant4: A simulation toolkit*, Nucl. Instrum. Meth. **A506** (2003) 250.

[33] M. Clemencic *et al.*, *The LHCb simulation application, Gauss: Design, evolution and experience*, J. Phys. Conf. Ser. **331** (2011) 032023.

[34] A. Rogozhnikov, *Reweighting with Boosted Decision Trees*, J. Phys. Conf. Ser. **762** (2016) , arXiv:1608.05806, https://github.com/arogozhnikov/hep_ml.

[35] LHCb collaboration, R. Aaij *et al.*, *Determination of the quark coupling strength* $|V_{ub}|$ *using baryonic decays*, Nature Physics **11** (2015) 743, arXiv:1504.01568.

[36] L. Anderlini *et al.*, *The PIDCalib package*, LHCb-PUB-2016-021, 2016.

[37] K. S. Cranmer, *Kernel estimation in high-energy physics*, Comput. Phys. Commun. **136** (2001) 198, arXiv:hep-ex/0011057.

[38] LHCb collaboration, R. Aaij *et al.*, *Measurement of the track reconstruction efficiency at LHCb*, JINST **10** (2015) P02007, arXiv:1408.1251.

[39] S. Tolk, J. Albrecht, F. Dettori, and A. Pellegrino, *Data driven trigger efficiency determination at LHCb*, LHCb-PUB-2014-039, 2014.

[40] LHCb collaboration, R. Aaij *et al.*, *Measurement of the b-quark production cross-section in 7 and 13 TeV pp collisions*, Phys. Rev. Lett. **118** (2017) 052002, arXiv:1612.05140, [Erratum: Phys. Rev. Lett.119,no.16,169901(2017)].

LHCb collaboration

R. Aaij[30], C. Abellán Beteta[47], T. Ackernley[57], B. Adeva[44], M. Adinolfi[51], H. Afsharnia[8], C.A. Aidala[78], S. Aiola[24], Z. Ajaltouni[8], S. Akar[62], P. Albicocco[21], J. Albrecht[13], F. Alessio[45], M. Alexander[56], A. Alfonso Albero[43], G. Alkhazov[36], P. Alvarez Cartelle[58], A.A. Alves Jr[44], S. Amato[2], Y. Amhis[10], L. An[20], L. Anderlini[20], G. Andreassi[46], M. Andreotti[19], F. Archilli[15], J. Arnau Romeu[9], A. Artamonov[42], M. Artuso[65], K. Arzymatov[40], E. Aslanides[9], M. Atzeni[47], B. Audurier[25], S. Bachmann[15], J.J. Back[53], S. Baker[58], V. Balagura[10,b], W. Baldini[19,45], A. Baranov[40], R.J. Barlow[59], S. Barsuk[10], W. Barter[58], M. Bartolini[22,45,h], F. Baryshnikov[74], G. Bassi[27], V. Batozskaya[34], B. Batsukh[65], A. Battig[13], A. Bay[46], M. Becker[13], F. Bedeschi[27], I. Bediaga[1], A. Beiter[65], L.J. Bel[30], V. Belavin[40], S. Belin[25], N. Beliy[4], V. Bellee[46], K. Belous[42], I. Belyaev[37], G. Bencivenni[21], E. Ben-Haim[11], S. Benson[30], S. Beranek[12], A. Berezhnoy[38], R. Bernet[47], D. Berninghoff[15], H.C. Bernstein[65], E. Bertholet[11], A. Bertolin[26], C. Betancourt[47], F. Betti[18,e], M.O. Bettler[52], Ia. Bezshyiko[47], S. Bhasin[51], J. Bhom[32], M.S. Bieker[13], S. Bifani[50], P. Billoir[11], A. Bizzeti[20,u], M. Bjørn[60], M.P. Blago[45], T. Blake[53], F. Blanc[46], S. Blusk[65], D. Bobulska[56], V. Bocci[29], O. Boente Garcia[44], T. Boettcher[61], A. Boldyrev[75], A. Bondar[41,x], N. Bondar[36], S. Borghi[59,45], M. Borisyak[40], M. Borsato[15], J.T. Borsuk[32], T.J.V. Bowcock[57], C. Bozzi[19], M.J. Bradley[58], S. Braun[15], A. Brea Rodriguez[44], M. Brodski[45], J. Brodzicka[32], A. Brossa Gonzalo[53], D. Brundu[25], E. Buchanan[51], A. Buonaura[47], C. Burr[45], A. Bursche[25], J.S. Butter[30], J. Buytaert[45], W. Byczynski[45], S. Cadeddu[25], H. Cai[69], R. Calabrese[19,g], L. Calero Diaz[21], S. Cali[21], R. Calladine[50], M. Calvi[23,i], M. Calvo Gomez[43,m], A. Camboni[43], P. Campana[21], D.H. Campora Perez[45], L. Capriotti[18,e], A. Carbone[18,e], G. Carboni[28], R. Cardinale[22,h], A. Cardini[25], P. Carniti[23,i], K. Carvalho Akiba[30], A. Casais Vidal[44], G. Casse[57], M. Cattaneo[45], G. Cavallero[45], R. Cenci[27,p], J. Cerasoli[9], M.G. Chapman[51], M. Charles[11,45], Ph. Charpentier[45], G. Chatzikonstantinidis[50], M. Chefdeville[7], V. Chekalina[40], C. Chen[3], S. Chen[25], A. Chernov[32], S.-G. Chitic[45], V. Chobanova[44], M. Chrzaszcz[32], A. Chubykin[36], P. Ciambrone[21], M.F. Cicala[53], X. Cid Vidal[44], G. Ciezarek[45], F. Cindolo[18], P.E.L. Clarke[55], M. Clemencic[45], H.V. Cliff[52], J. Closier[45], J.L. Cobbledick[59], V. Coco[45], J.A.B. Coelho[10], J. Cogan[9], E. Cogneras[8], L. Cojocariu[35], P. Collins[45], T. Colombo[45], A. Comerma-Montells[15], A. Contu[25], N. Cooke[50], G. Coombs[56], S. Coquereau[43], G. Corti[45], C.M. Costa Sobral[53], B. Couturier[45], D.C. Craik[61], J. Crkovska[64], A. Crocombe[53], M. Cruz Torres[1], R. Currie[55], C.L. Da Silva[64], E. Dall'Occo[30], J. Dalseno[44,51], C. D'Ambrosio[45], A. Danilina[37], P. d'Argent[15], A. Davis[59], O. De Aguiar Francisco[45], K. De Bruyn[45], S. De Capua[59], M. De Cian[46], J.M. De Miranda[1], L. De Paula[2], M. De Serio[17,d], P. De Simone[21], J.A. de Vries[30], C.T. Dean[64], W. Dean[78], D. Decamp[7], L. Del Buono[11], B. Delaney[52], H.-P. Dembinski[14], M. Demmer[13], A. Dendek[33], V. Denysenko[47], D. Derkach[75], O. Deschamps[8], F. Desse[10], F. Dettori[25], B. Dey[6], A. Di Canto[45], P. Di Nezza[21], S. Didenko[74], H. Dijkstra[45], V. Dobishuk[49], F. Dordei[25], M. Dorigo[27,y], A.C. dos Reis[1], L. Douglas[56], A. Dovbnya[48], K. Dreimanis[57], M.W. Dudek[32], L. Dufour[45], G. Dujany[11], P. Durante[45], J.M. Durham[64], D. Dutta[59], R. Dzhelyadin[42,†], M. Dziewiecki[15], A. Dziurda[32], A. Dzyuba[36], S. Easo[54], U. Egede[58], V. Egorychev[37], S. Eidelman[41,x], S. Eisenhardt[55], R. Ekelhof[13], S. Ek-In[46], L. Eklund[56], S. Ely[65], A. Ene[35], S. Escher[12], S. Esen[30], T. Evans[45], A. Falabella[18], J. Fan[3], N. Farley[50], S. Farry[57], D. Fazzini[10], M. Féo[45], P. Fernandez Declara[45], A. Fernandez Prieto[44], F. Ferrari[18,e], L. Ferreira Lopes[46], F. Ferreira Rodrigues[2], S. Ferreres Sole[30], M. Ferrillo[47], M. Ferro-Luzzi[45], S. Filippov[39], R.A. Fini[17], M. Fiorini[19,g], M. Firlej[33], K.M. Fischer[60], C. Fitzpatrick[45], T. Fiutowski[33], F. Fleuret[10,b], M. Fontana[45], F. Fontanelli[22,h], R. Forty[45], V. Franco Lima[57], M. Franco Sevilla[63], M. Frank[45], C. Frei[45], D.A. Friday[56], J. Fu[24,q], M. Fuehring[13], W. Funk[45], E. Gabriel[55], A. Gallas Torreira[44], D. Galli[18,e], S. Gallorini[26], S. Gambetta[55], Y. Gan[3], M. Gandelman[2], P. Gandini[24], Y. Gao[3], L.M. Garcia Martin[77], J. García Pardiñas[47], B. Garcia Plana[44], F.A. Garcia Rosales[10], J. Garra Tico[52], L. Garrido[43],

D. Gascon[43], C. Gaspar[45], D. Gerick[15], E. Gersabeck[59], M. Gersabeck[59], T. Gershon[53], D. Gerstel[9], Ph. Ghez[7], V. Gibson[52], A. Gioventù[44], O.G. Girard[46], P. Gironella Gironell[43], L. Giubega[35], C. Giugliano[19], K. Gizdov[55], V.V. Gligorov[11], C. Göbel[67], D. Golubkov[37], A. Golutvin[58,74], A. Gomes[1,a], P. Gorbounov[37,5], I.V. Gorelov[38], C. Gotti[23,i], E. Govorkova[30], J.P. Grabowski[15], R. Graciani Diaz[43], T. Grammatico[11], L.A. Granado Cardoso[45], E. Graugés[43], E. Graverini[46], G. Graziani[20], A. Grecu[35], R. Greim[30], P. Griffith[19], L. Grillo[59], L. Gruber[45], B.R. Gruberg Cazon[60], C. Gu[3], E. Gushchin[39], A. Guth[12], Yu. Guz[42,45], T. Gys[45], T. Hadavizadeh[60], G. Haefeli[46], C. Haen[45], S.C. Haines[52], P.M. Hamilton[63], Q. Han[6], X. Han[15], T.H. Hancock[60], S. Hansmann-Menzemer[15], N. Harnew[60], T. Harrison[57], R. Hart[30], C. Hasse[45], M. Hatch[45], J. He[4], M. Hecker[58], K. Heijhoff[30], K. Heinicke[13], A. Heister[13], A.M. Hennequin[45], K. Hennessy[57], L. Henry[77], J. Heuel[12], A. Hicheur[66], R. Hidalgo Charman[59], D. Hill[60], M. Hilton[59], P.H. Hopchev[46], J. Hu[15], W. Hu[6], W. Huang[4], W. Hulsbergen[30], T. Humair[58], R.J. Hunter[53], M. Hushchyn[75], D. Hutchcroft[57], D. Hynds[30], P. Ibis[13], M. Idzik[33], P. Ilten[50], A. Inglessi[36], A. Inyakin[42], K. Ivshin[36], R. Jacobsson[45], S. Jakobsen[45], J. Jalocha[60], E. Jans[30], B.K. Jashal[77], A. Jawahery[63], V. Jevtic[13], F. Jiang[3], M. John[60], D. Johnson[45], C.R. Jones[52], B. Jost[45], N. Jurik[60], S. Kandybei[48], M. Karacson[45], J.M. Kariuki[51], N. Kazeev[75], M. Kecke[15], F. Keizer[52,52], M. Kelsey[65], M. Kenzie[52], T. Ketel[31], B. Khanji[45], A. Kharisova[76], K.E. Kim[65], T. Kirn[12], V.S. Kirsebom[46], S. Klaver[21], K. Klimaszewski[34], S. Koliiev[49], A. Kondybayeva[74], A. Konoplyannikov[37], P. Kopciewicz[33], R. Kopecna[15], P. Koppenburg[30], I. Kostiuk[30,49], O. Kot[49], S. Kotriakhova[36], L. Kravchuk[39], R.D. Krawczyk[45], M. Kreps[53], F. Kress[58], S. Kretzschmar[12], P. Krokovny[41,x], W. Krupa[33], W. Krzemien[34], W. Kucewicz[32,l], M. Kucharczyk[32], V. Kudryavtsev[41,x], H.S. Kuindersma[30], G.J. Kunde[64], T. Kvaratskheliya[37], D. Lacarrere[45], G. Lafferty[59], A. Lai[25], D. Lancierini[47], J.J. Lane[59], G. Lanfranchi[21], C. Langenbruch[12], T. Latham[53], F. Lazzari[27,v], C. Lazzeroni[50], R. Le Gac[9], R. Lefèvre[8], A. Leflat[38], F. Lemaitre[45], O. Leroy[9], T. Lesiak[32], B. Leverington[15], H. Li[68], X. Li[64], Y. Li[5], Z. Li[65], X. Liang[65], R. Lindner[45], V. Lisovskyi[10], G. Liu[68], X. Liu[3], D. Loh[53], A. Loi[25], J. Lomba Castro[44], I. Longstaff[56], J.H. Lopes[2], G. Loustau[47], G.H. Lovell[52], Y. Lu[5], D. Lucchesi[26,o], M. Lucio Martinez[30], Y. Luo[3], A. Lupato[26], E. Luppi[19,g], O. Lupton[53], A. Lusiani[27], X. Lyu[4], S. Maccolini[18,e], F. Machefert[10], F. Maciuc[35], V. Macko[46], P. Mackowiak[13], S. Maddrell-Mander[51], L.R. Madhan Mohan[51], O. Maev[36,45], A. Maevskiy[75], D. Maisuzenko[36], M.W. Majewski[33], S. Malde[60], B. Malecki[45], A. Malinin[73], T. Maltsev[41,x], H. Malygina[15], G. Manca[25,f], G. Mancinelli[9], R. Manera Escalero[43], D. Manuzzi[18,e], D. Marangotto[24,q], J. Maratas[8,w], J.F. Marchand[7], U. Marconi[18], S. Mariani[20], C. Marin Benito[10], M. Marinangeli[46], P. Marino[46], J. Marks[15], P.J. Marshall[57], G. Martellotti[29], L. Martinazzoli[45], M. Martinelli[23], D. Martinez Santos[44], F. Martinez Vidal[77], A. Massafferri[1], M. Materok[12], R. Matev[45], A. Mathad[47], Z. Mathe[45], V. Matiunin[37], C. Matteuzzi[23], K.R. Mattioli[78], A. Mauri[47], E. Maurice[10,b], M. McCann[58,45], L. Mcconnell[16], A. McNab[59], R. McNulty[16], J.V. Mead[57], B. Meadows[62], C. Meaux[9], G. Meier[13], N. Meinert[71], D. Melnychuk[34], S. Meloni[23,i], M. Merk[30], A. Merli[24], M. Mikhasenko[45], D.A. Milanes[70], E. Millard[53], M.-N. Minard[7], O. Mineev[37], L. Minzoni[19,g], S.E. Mitchell[55], B. Mitreska[59], D.S. Mitzel[45], A. Mödden[13], A. Mogini[11], R.D. Moise[58], T. Mombächer[13], I.A. Monroy[70], S. Monteil[8], M. Morandin[26], G. Morello[21], M.J. Morello[27,t], J. Moron[33], A.B. Morris[9], A.G. Morris[53], R. Mountain[65], H. Mu[3], F. Muheim[55], M. Mukherjee[6], M. Mulder[30], D. Müller[45], K. Müller[47], V. Müller[13], C.H. Murphy[60], D. Murray[59], P. Muzzetto[25], P. Naik[51], T. Nakada[46], R. Nandakumar[54], A. Nandi[60], T. Nanut[46], I. Nasteva[2], M. Needham[55], N. Neri[24,q], S. Neubert[15], N. Neufeld[45], R. Newcombe[58], T.D. Nguyen[46], C. Nguyen-Mau[46,n], E.M. Niel[10], S. Nieswand[12], N. Nikitin[38], N.S. Nolte[45], C. Nunez[78], A. Oblakowska-Mucha[33], V. Obraztsov[42], S. Ogilvy[56], D.P. O'Hanlon[18], R. Oldeman[25,f], C.J.G. Onderwater[72], J. D. Osborn[78], A. Ossowska[32], J.M. Otalora Goicochea[2], T. Ovsiannikova[37], P. Owen[47], A. Oyanguren[77], P.R. Pais[46], T. Pajero[27,t], A. Palano[17], M. Palutan[21], G. Panshin[76], A. Papanestis[54],

M. Pappagallo[55], L.L. Pappalardo[19,g], C. Pappenheimer[62], W. Parker[63], C. Parkes[59], G. Passaleva[20,45], A. Pastore[17], M. Patel[58], C. Patrignani[18,e], A. Pearce[45], A. Pellegrino[30], M. Pepe Altarelli[45], S. Perazzini[18], D. Pereima[37], P. Perret[8], L. Pescatore[46], K. Petridis[51], A. Petrolini[22,h], A. Petrov[73], S. Petrucci[55], M. Petruzzo[24,q], B. Pietrzyk[7], G. Pietrzyk[46], M. Pikies[32], M. Pili[60], D. Pinci[29], J. Pinzino[45], F. Pisani[45], A. Piucci[15], V. Placinta[35], S. Playfer[55], J. Plews[50], M. Plo Casasus[44], F. Polci[11], M. Poli Lener[21], M. Poliakova[65], A. Poluektov[9], N. Polukhina[74,c], I. Polyakov[65], E. Polycarpo[2], G.J. Pomery[51], S. Ponce[45], A. Popov[42], D. Popov[50], S. Poslavskii[42], K. Prasanth[32], L. Promberger[45], C. Prouve[44], V. Pugatch[49], A. Puig Navarro[47], H. Pullen[60], G. Punzi[27,p], W. Qian[4], J. Qin[4], R. Quagliani[11], B. Quintana[8], N.V. Raab[16], R.I. Rabadan Trejo[9], B. Rachwal[33], J.H. Rademacker[51], M. Rama[27], M. Ramos Pernas[44], M.S. Rangel[2], F. Ratnikov[40,75], G. Raven[31], M. Reboud[7], F. Redi[46], F. Reiss[11], C. Remon Alepuz[77], Z. Ren[3], V. Renaudin[60], S. Ricciardi[54], S. Richards[51], K. Rinnert[57], P. Robbe[10], A. Robert[11], A.B. Rodrigues[46], E. Rodrigues[62], J.A. Rodriguez Lopez[70], M. Roehrken[45], S. Roiser[45], A. Rollings[60], V. Romanovskiy[42], M. Romero Lamas[44], A. Romero Vidal[44], J.D. Roth[78], M. Rotondo[21], M.S. Rudolph[65], T. Ruf[45], J. Ruiz Vidal[77], J. Ryzka[33], J.J. Saborido Silva[44], N. Sagidova[36], B. Saitta[25,f], C. Sanchez Gras[30], C. Sanchez Mayordomo[77], B. Sanmartin Sedes[44], R. Santacesaria[29], C. Santamarina Rios[44], M. Santimaria[21], E. Santovetti[28,j], G. Sarpis[59], A. Sarti[29], C. Satriano[29,s], A. Satta[28], M. Saur[4], D. Savrina[37,38], L.G. Scantlebury Smead[60], S. Schael[12], M. Schellenberg[13], M. Schiller[56], H. Schindler[45], M. Schmelling[14], T. Schmelzer[13], B. Schmidt[45], O. Schneider[46], A. Schopper[45], H.F. Schreiner[62], M. Schubiger[30], S. Schulte[46], M.H. Schune[10], R. Schwemmer[45], B. Sciascia[21], A. Sciubba[29,k], S. Sellam[66], A. Semennikov[37], A. Sergi[50,45], N. Serra[47], J. Serrano[9], L. Sestini[26], A. Seuthe[13], P. Seyfert[45], D.M. Shangase[78], M. Shapkin[42], T. Shears[57], L. Shekhtman[41,x], V. Shevchenko[73,74], E. Shmanin[74], J.D. Shupperd[65], B.G. Siddi[19], R. Silva Coutinho[47], L. Silva de Oliveira[2], G. Simi[26,o], S. Simone[17,d], I. Skiba[19], N. Skidmore[15], T. Skwarnicki[65], M.W. Slater[50], J.G. Smeaton[52], A. Smetkina[37], E. Smith[12], I.T. Smith[55], M. Smith[58], A. Snoch[30], M. Soares[18], L. Soares Lavra[1], M.D. Sokoloff[62], F.J.P. Soler[56], B. Souza De Paula[2], B. Spaan[13], E. Spadaro Norella[24,q], P. Spradlin[56], F. Stagni[45], M. Stahl[62], S. Stahl[45], P. Stefko[46], S. Stefkova[58], O. Steinkamp[47], S. Stemmle[15], O. Stenyakin[42], M. Stepanova[36], H. Stevens[13], A. Stocchi[10], S. Stone[65], S. Stracka[27], M.E. Stramaglia[46], M. Straticiuc[35], S. Strokov[76], J. Sun[3], L. Sun[69], Y. Sun[63], P. Svihra[59], K. Swientek[33], A. Szabelski[34], T. Szumlak[33], M. Szymanski[4], S. Taneja[59], Z. Tang[3], T. Tekampe[13], G. Tellarini[19], F. Teubert[45], E. Thomas[45], K.A. Thomson[57], M.J. Tilley[58], V. Tisserand[8], S. T'Jampens[7], M. Tobin[5], S. Tolk[45], L. Tomassetti[19,g], D. Tonelli[27], D.Y. Tou[11], E. Tournefier[7], M. Traill[56], M.T. Tran[46], C. Trippl[46], A. Trisovic[52], A. Tsaregorodtsev[9], G. Tuci[27,45,p], A. Tully[46], N. Tuning[30], A. Ukleja[34], A. Usachov[10], A. Ustyuzhanin[40,75], U. Uwer[15], A. Vagner[76], V. Vagnoni[18], A. Valassi[45], G. Valenti[18], M. van Beuzekom[30], H. Van Hecke[64], E. van Herwijnen[45], C.B. Van Hulse[16], M. van Veghel[72], R. Vazquez Gomez[43], P. Vazquez Regueiro[44], C. Vázquez Sierra[30], S. Vecchi[19], J.J. Velthuis[51], M. Veltri[20,r], A. Venkateswaran[65], M. Vernet[8], M. Veronesi[30], M. Vesterinen[53], J.V. Viana Barbosa[45], D. Vieira[4], M. Vieites Diaz[46], H. Viemann[71], X. Vilasis-Cardona[43,m], A. Vitkovskiy[30], V. Volkov[38], A. Vollhardt[47], D. Vom Bruch[11], A. Vorobyev[36], V. Vorobyev[41,x], N. Voropaev[36], R. Waldi[71], J. Walsh[27], J. Wang[3], J. Wang[69], J. Wang[5], M. Wang[3], Y. Wang[6], Z. Wang[47], D.R. Ward[52], H.M. Wark[57], N.K. Watson[50], D. Websdale[58], A. Weiden[47], C. Weisser[61], B.D.C. Westhenry[51], D.J. White[59], M. Whitehead[12], D. Wiedner[13], G. Wilkinson[60], M. Wilkinson[65], I. Williams[52], M. Williams[61], M.R.J. Williams[59], T. Williams[50], F.F. Wilson[54], M. Winn[10], W. Wislicki[34], M. Witek[32], G. Wormser[10], S.A. Wotton[52], H. Wu[65], K. Wyllie[45], Z. Xiang[4], D. Xiao[6], Y. Xie[6], H. Xing[68], A. Xu[3], L. Xu[3], M. Xu[6], Q. Xu[4], Z. Xu[7], Z. Xu[3], Z. Yang[3], Z. Yang[63], Y. Yao[65], L.E. Yeomans[57], H. Yin[6], J. Yu[6,aa], X. Yuan[65], O. Yushchenko[42], K.A. Zarebski[50], M. Zavertyaev[14,c], M. Zdybal[32], M. Zeng[3], D. Zhang[6],

L. Zhang[3], S. Zhang[3], W.C. Zhang[3,z], Y. Zhang[45], A. Zhelezov[15], Y. Zheng[4], X. Zhou[4], Y. Zhou[4], X. Zhu[3], V. Zhukov[12,38], J.B. Zonneveld[55], S. Zucchelli[18,e].

[1] *Centro Brasileiro de Pesquisas Físicas (CBPF), Rio de Janeiro, Brazil*
[2] *Universidade Federal do Rio de Janeiro (UFRJ), Rio de Janeiro, Brazil*
[3] *Center for High Energy Physics, Tsinghua University, Beijing, China*
[4] *University of Chinese Academy of Sciences, Beijing, China*
[5] *Institute Of High Energy Physics (IHEP), Beijing, China*
[6] *Institute of Particle Physics, Central China Normal University, Wuhan, Hubei, China*
[7] *Univ. Grenoble Alpes, Univ. Savoie Mont Blanc, CNRS, IN2P3-LAPP, Annecy, France*
[8] *Université Clermont Auvergne, CNRS/IN2P3, LPC, Clermont-Ferrand, France*
[9] *Aix Marseille Univ, CNRS/IN2P3, CPPM, Marseille, France*
[10] *LAL, Univ. Paris-Sud, CNRS/IN2P3, Université Paris-Saclay, Orsay, France*
[11] *LPNHE, Sorbonne Université, Paris Diderot Sorbonne Paris Cité, CNRS/IN2P3, Paris, France*
[12] *I. Physikalisches Institut, RWTH Aachen University, Aachen, Germany*
[13] *Fakultät Physik, Technische Universität Dortmund, Dortmund, Germany*
[14] *Max-Planck-Institut für Kernphysik (MPIK), Heidelberg, Germany*
[15] *Physikalisches Institut, Ruprecht-Karls-Universität Heidelberg, Heidelberg, Germany*
[16] *School of Physics, University College Dublin, Dublin, Ireland*
[17] *INFN Sezione di Bari, Bari, Italy*
[18] *INFN Sezione di Bologna, Bologna, Italy*
[19] *INFN Sezione di Ferrara, Ferrara, Italy*
[20] *INFN Sezione di Firenze, Firenze, Italy*
[21] *INFN Laboratori Nazionali di Frascati, Frascati, Italy*
[22] *INFN Sezione di Genova, Genova, Italy*
[23] *INFN Sezione di Milano-Bicocca, Milano, Italy*
[24] *INFN Sezione di Milano, Milano, Italy*
[25] *INFN Sezione di Cagliari, Monserrato, Italy*
[26] *INFN Sezione di Padova, Padova, Italy*
[27] *INFN Sezione di Pisa, Pisa, Italy*
[28] *INFN Sezione di Roma Tor Vergata, Roma, Italy*
[29] *INFN Sezione di Roma La Sapienza, Roma, Italy*
[30] *Nikhef National Institute for Subatomic Physics, Amsterdam, Netherlands*
[31] *Nikhef National Institute for Subatomic Physics and VU University Amsterdam, Amsterdam, Netherlands*
[32] *Henryk Niewodniczanski Institute of Nuclear Physics Polish Academy of Sciences, Kraków, Poland*
[33] *AGH - University of Science and Technology, Faculty of Physics and Applied Computer Science, Kraków, Poland*
[34] *National Center for Nuclear Research (NCBJ), Warsaw, Poland*
[35] *Horia Hulubei National Institute of Physics and Nuclear Engineering, Bucharest-Magurele, Romania*
[36] *Petersburg Nuclear Physics Institute NRC Kurchatov Institute (PNPI NRC KI), Gatchina, Russia*
[37] *Institute of Theoretical and Experimental Physics NRC Kurchatov Institute (ITEP NRC KI), Moscow, Russia, Moscow, Russia*
[38] *Institute of Nuclear Physics, Moscow State University (SINP MSU), Moscow, Russia*
[39] *Institute for Nuclear Research of the Russian Academy of Sciences (INR RAS), Moscow, Russia*
[40] *Yandex School of Data Analysis, Moscow, Russia*
[41] *Budker Institute of Nuclear Physics (SB RAS), Novosibirsk, Russia*
[42] *Institute for High Energy Physics NRC Kurchatov Institute (IHEP NRC KI), Protvino, Russia, Protvino, Russia*
[43] *ICCUB, Universitat de Barcelona, Barcelona, Spain*
[44] *Instituto Galego de Física de Altas Enerxías (IGFAE), Universidade de Santiago de Compostela, Santiago de Compostela, Spain*
[45] *European Organization for Nuclear Research (CERN), Geneva, Switzerland*
[46] *Institute of Physics, Ecole Polytechnique Fédérale de Lausanne (EPFL), Lausanne, Switzerland*
[47] *Physik-Institut, Universität Zürich, Zürich, Switzerland*
[48] *NSC Kharkiv Institute of Physics and Technology (NSC KIPT), Kharkiv, Ukraine*
[49] *Institute for Nuclear Research of the National Academy of Sciences (KINR), Kyiv, Ukraine*

[50] University of Birmingham, Birmingham, United Kingdom
[51] H.H. Wills Physics Laboratory, University of Bristol, Bristol, United Kingdom
[52] Cavendish Laboratory, University of Cambridge, Cambridge, United Kingdom
[53] Department of Physics, University of Warwick, Coventry, United Kingdom
[54] STFC Rutherford Appleton Laboratory, Didcot, United Kingdom
[55] School of Physics and Astronomy, University of Edinburgh, Edinburgh, United Kingdom
[56] School of Physics and Astronomy, University of Glasgow, Glasgow, United Kingdom
[57] Oliver Lodge Laboratory, University of Liverpool, Liverpool, United Kingdom
[58] Imperial College London, London, United Kingdom
[59] Department of Physics and Astronomy, University of Manchester, Manchester, United Kingdom
[60] Department of Physics, University of Oxford, Oxford, United Kingdom
[61] Massachusetts Institute of Technology, Cambridge, MA, United States
[62] University of Cincinnati, Cincinnati, OH, United States
[63] University of Maryland, College Park, MD, United States
[64] Los Alamos National Laboratory (LANL), Los Alamos, United States
[65] Syracuse University, Syracuse, NY, United States
[66] Laboratory of Mathematical and Subatomic Physics , Constantine, Algeria, associated to [2]
[67] Pontifícia Universidade Católica do Rio de Janeiro (PUC-Rio), Rio de Janeiro, Brazil, associated to [2]
[68] South China Normal University, Guangzhou, China, associated to [3]
[69] School of Physics and Technology, Wuhan University, Wuhan, China, associated to [3]
[70] Departamento de Fisica , Universidad Nacional de Colombia, Bogota, Colombia, associated to [11]
[71] Institut für Physik, Universität Rostock, Rostock, Germany, associated to [15]
[72] Van Swinderen Institute, University of Groningen, Groningen, Netherlands, associated to [30]
[73] National Research Centre Kurchatov Institute, Moscow, Russia, associated to [37]
[74] National University of Science and Technology "MISIS", Moscow, Russia, associated to [37]
[75] National Research University Higher School of Economics, Moscow, Russia, associated to [40]
[76] National Research Tomsk Polytechnic University, Tomsk, Russia, associated to [37]
[77] Instituto de Fisica Corpuscular, Centro Mixto Universidad de Valencia - CSIC, Valencia, Spain, associated to [43]
[78] University of Michigan, Ann Arbor, United States, associated to [65]

[a] Universidade Federal do Triângulo Mineiro (UFTM), Uberaba-MG, Brazil
[b] Laboratoire Leprince-Ringuet, Palaiseau, France
[c] P.N. Lebedev Physical Institute, Russian Academy of Science (LPI RAS), Moscow, Russia
[d] Università di Bari, Bari, Italy
[e] Università di Bologna, Bologna, Italy
[f] Università di Cagliari, Cagliari, Italy
[g] Università di Ferrara, Ferrara, Italy
[h] Università di Genova, Genova, Italy
[i] Università di Milano Bicocca, Milano, Italy
[j] Università di Roma Tor Vergata, Roma, Italy
[k] Università di Roma La Sapienza, Roma, Italy
[l] AGH - University of Science and Technology, Faculty of Computer Science, Electronics and Telecommunications, Kraków, Poland
[m] LIFAELS, La Salle, Universitat Ramon Llull, Barcelona, Spain
[n] Hanoi University of Science, Hanoi, Vietnam
[o] Università di Padova, Padova, Italy
[p] Università di Pisa, Pisa, Italy
[q] Università degli Studi di Milano, Milano, Italy
[r] Università di Urbino, Urbino, Italy
[s] Università della Basilicata, Potenza, Italy
[t] Scuola Normale Superiore, Pisa, Italy
[u] Università di Modena e Reggio Emilia, Modena, Italy
[v] Università di Siena, Siena, Italy
[w] MSU - Iligan Institute of Technology (MSU-IIT), Iligan, Philippines
[x] Novosibirsk State University, Novosibirsk, Russia
[y] Sezione INFN di Trieste, Trieste, Italy

[z] School of Physics and Information Technology, Shaanxi Normal University (SNNU), Xi'an, China
[aa] Physics and Micro Electronic College, Hunan University, Changsha City, China

[†] Deceased